



Influence of amorphous phase on coercivity in SmCo₅-Cu nanocomposites

Franziska Staab^{a,1}, Yangyiwei Yang^{b,*,1}, Eren Foya^b, Enrico Bruder^a, Benjamin Zingsem^{c,d}, Esmaeil Adabifiroozjahi^e, Despoina Nasiou^e, Konstantin Skokov^f, David Koch^g, Michael Farle^c, Rafal E. Dunin-Borkowski^d, Leopoldo Molina-Luna^e, Oliver Gutfleisch^{f,2}, Bai-Xiang Xu^b, Karsten Durst^a

^a Physical Metallurgy (PhM), Materials Science Department, Technical University of Darmstadt, Peter-Grünberg-Str. 2, 64287 Darmstadt, Germany

^b Mechanics of Functional Materials (MFM), Materials Science Department, Technical University of Darmstadt, Otto-Berndt-Str. 3, 64287 Darmstadt, Germany

^c Faculty of Physics and Center for Nanointegration (CENIDE), University of Duisburg-Essen, 47057 Duisburg, Germany

^d Ernst Ruska-Centre for Microscopy and Spectroscopy with Electrons and Peter Grünberg Institute, Forschungszentrum Jülich GmbH, 52425 Jülich, Germany

^e Advanced Electron Microscopy (AEM), Materials Science Department, Technical University of Darmstadt, Peter-Grünberg-Str. 2, 64287 Darmstadt, Germany

^f Functional Materials (FM), Materials Science Department, Technical University of Darmstadt, Peter-Grünberg-Str. 16, 64287 Darmstadt, Germany

^g Structure Research, Materials Science Department, Technical University of Darmstadt, Peter-Grünberg-Str. 2, 64287 Darmstadt, Germany

ARTICLE INFO

Keywords:

SmCo₅-Cu nanocomposites
Severe plastic deformation
High-pressure torsion
Micromagnetic simulation
Amorphous SmCo₅

ABSTRACT

Severe plastic deformation of powder blends consisting of SmCo₅-Cu results in magnetically hardened nanocomposite bulk materials. Previously it was reported that the microstructure is continuously refined with increasing deformation, yet, coercivity saturates at a certain level of strain and partial amorphization of the SmCo₅ phase is observed. In this work larger strains, over the range of the previous work are applied showing further structural refinement but a strong decrease in coercivity. Micromagnetic simulations based on the experimentally observed microstructure serve to clarify the effect of amorphization in the SmCo₅ phase and disclose the detrimental character of the amorphous phase. For a fixed volume fraction of nanocrystals the simulations reveal an increasing coercivity with decreasing the size of them due to increasing number of interfaces acting as pinning sites. Furthermore, our micromagnetic simulations disclose the mechanisms of saturation and decline of magnetic hardening due to the strain induced by high-pressure torsion.

As the demand for renewable energy sources increases, the demand for high-performance permanent magnets is also rising [1]. In order to fulfill the requirements for suitable hard magnetic materials, good intrinsic magnetic properties need to be combined with optimized extrinsic magnetic properties, notably the remanent magnetization M_r and the coercivity H_c . Therefore, the micro- or nanostructure need to be adjusted accordingly. The conventional processing techniques for permanent magnets are based on a powder-metallurgical sintering route [2]. It has been shown that the coercivity of such magnets usually does not exceed 20–30% of the theoretical prediction of $H_c = 2K_u/\mu_0 M_s$ (K_u as the 1st magnetocrystalline uniaxial anisotropy constant, μ_0 as the vacuum permeability, and M_s as the saturated magnetization) given by the Stoner-Wohlfarth model for a magnetic field applied along the easy

direction [3,2]. Hence, it is challenging to develop a technology to adjust the nano- or microstructure of bulk magnetic materials.

Severe plastic deformation such as high-pressure torsion (HPT) is a well-known top-down approach to generate ultrafine-grained materials [4,5]. Recently it has been shown that HPT applied to powder blends is a promising process for the production of textured nanocomposite hard magnetic materials [6–9]. However, the process was also applied to several different other soft- and hard-magnetic material systems (bulk and powders), ranging from pure elements such as iron or cobalt, to nanocomposites, high entropy alloys and hard magnetic systems such as Nd-Fe-B and Sm-Fe-N. More details of the HPT process applied to magnetic materials can be found in recent review papers [9,10]. Applying the HPT process to powder blends allows the free selection of

* Corresponding author.

E-mail address: yangyiwei.yang@mfm.tu-darmstadt.de (Y. Yang).

¹ Authors contributed equally.

² Oliver Gutfleisch was an Editor of the journal during the review period of the article. To avoid a conflict of interest, Oliver Gutfleisch was blinded to the record and another editor processed this manuscript.

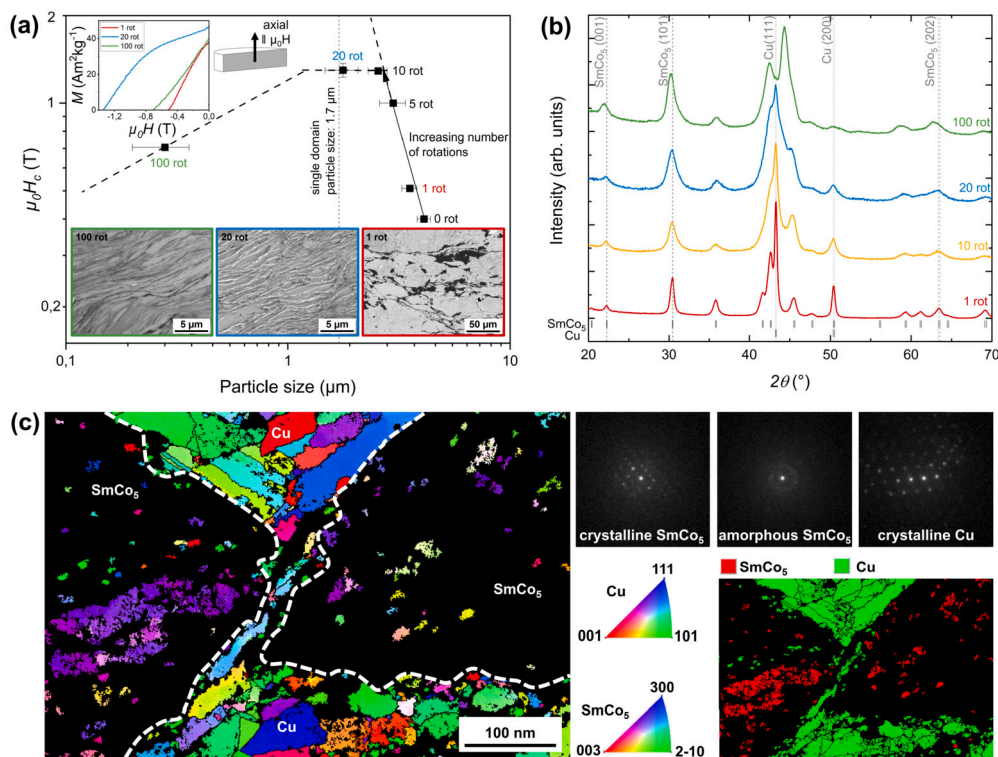


Fig. 1. (a) Coercivity as a function of the particle size with insets of the room temperature magnetic hysteresis curves measured in axial direction and SEM-BSE images of the cross section of the HPT-deformed samples subjected to 1, 20 (adapted from [6] with permission) and 100 rotations, (b) XRD diffractograms, (c) 4D-SPED orientation and phase map of a HPT-deformed sample subjected to 20 rotations showing two SmCo_5 particles containing nanocrystallites in an amorphous matrix, separated by a Cu-layer. Diffraction patterns are shown for crystalline and amorphous SmCo_5 and for Cu.

the magnetic phase and the grain boundary phase, without limitation of phase formations as in the case of the powder-metallurgical sintering route. In addition, HPT enables the adjustment of the microstructure by parameter variation such as the applied strain, pressure and temperature [6,7,9]. However, the microstructural effects on the magnetization reversal behavior at small length scales are very difficult to access experimentally.

Recently, micromagnetic modeling has been successful in simulating magnetization dynamics under various stimuli such as magnetic, elastic, and thermal fields. It has been widely employed in examining the role of microstructural features on magnetic reversal mechanisms, that is domain nucleation and domain wall pinning [11,12]. Up to date, micromagnetic simulations have been successfully performed on various microstructures of permanent magnets, notably, the nanoscopic granular [13–15] and cellular structures [12], in which various structural features, such as the grain shape [11,16,17], aspect ratio [18], and misalignment [13] have been examined and discussed. However, the microstructural evolution of nanocomposites, produced by severe plastic deformation, has been rarely modeled. Previously, an increasing coercivity with increasing strain was reported followed by a saturation above 10 HPT rotations [6]. In this work we further increase the degree of deformation and investigate the microstructural changes and magnetic properties. An emphasis is put on micromagnetic simulations that are reflecting experimentally observed microstructural features, to clarify the role of partial amorphization on in HPT processed SmCo_5 -Cu nanocomposites.

The nanocomposites of SmCo_5 and Cu were produced by high-pressure torsion of a powder blend consisting of 80 wt.% intermetallic fine-grained powder of SmCo_5 (Alfa Aesar) and 20 wt.% of Cu powder (99.9%, Alfa Aesar). For this work a sample subjected to 100 rotations was prepared, whereas the samples subjected to 1, 10 and 20 rotations were taken from previous work [6]. Experimental details as well as details of the investigation by microstructural, X-ray diffraction (XRD) and

magnetic analyses can be found in [6] and in Supplementary Note 1. From the sample subjected to 20 rotations a lamella was prepared from a region showing strong microstructural refinement. TEM analyses was performed by 4D scanning precession electron diffraction (SPED) on a JOEL ARM-200F TEM (further experimental details and operation parameters can be found in Supplementary Note 1).

In Fig. 1a the coercivity is plotted as a function of the particle size. H_c increases with a reduction in particle size for the samples subjected to up to 10 rotations. This increase is predominantly related to the particle refinement in combination with thin Cu-layers in between the ferromagnetic particles with a sufficient thickness for magnetic decoupling [6,19]. With further increase of strain up to 20 rotations H_c remains nearly constant even though the particle size further decreases and reaches the single domain size of $l = 1.7 \mu\text{m}$ [20]. Therefore, a further increase of coercivity is expected, indicated by the dashed line. After 100 rotations the particle size is further diminished, but the coercivity strongly decreases to 0.71 T. The second quadrant of the $M(H)$ hysteresis curves, which was used to determine the coercivities can be found as an inset. The microstructures of the SmCo_5 -Cu nanocomposites subjected to 1, 20 and 100 rotations obtained by BSE imaging, shown as an inset, reveal a refinement with increasing number of rotations. After 20 and 100 rotations, the SmCo_5 particles show a strong elongation perpendicular to the direction of applied pressure while the particles are well surrounded by the diamagnetic fcc Cu-phase.

XRD analyses depicted in Fig. 1b reveals a pronounced peak broadening with increasing number of rotations due to grain refinement and partial amorphization of the SmCo_5 phase on a macroscopic length scale as indicated by TEM Fig. 1c. The intensity of Cu-reflexes such as (111)- and (200)-decreases for the sample subjected to 100 rotations and the positions of the SmCo_5 -reflexes are slightly shifted to smaller angles. This shift implies an increased lattice parameter c indicating that some copper gets dissolved in the SmCo_5 phase forming $\text{SmCo}_{5-x}\text{Cu}_x$ [21] via mechanical alloying. SPED investigations by ACOM (Fig. 1c) provide a

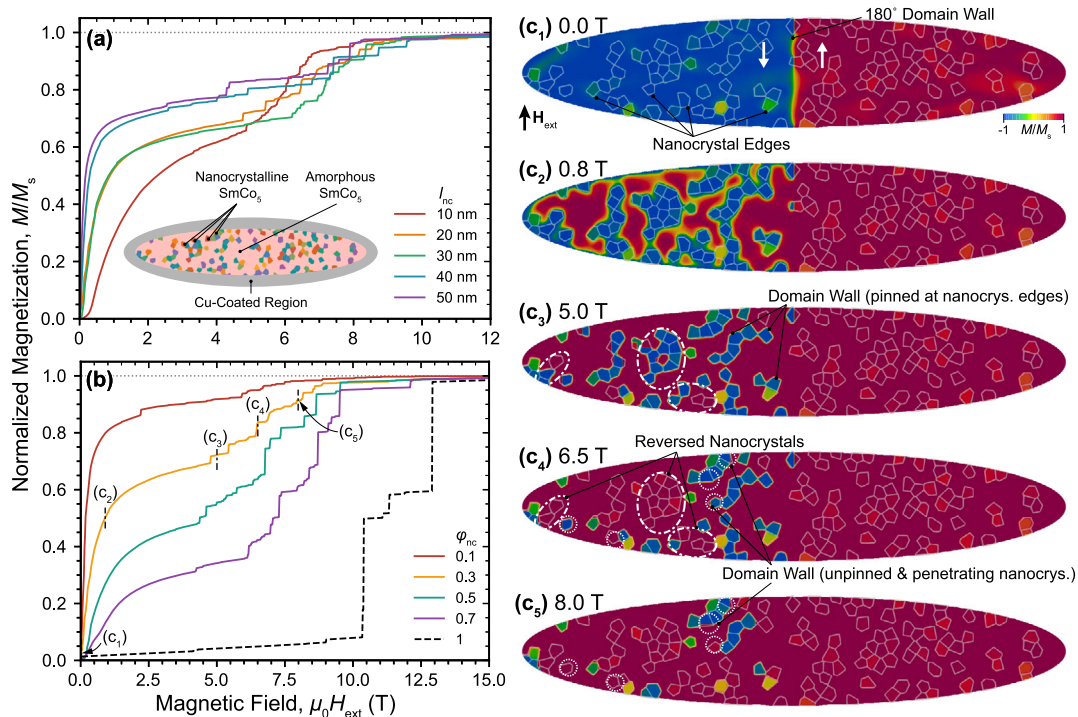


Fig. 2. Simulated initial hysteresis curves for (a) varying nanocrystal size l_{nc} with constant volume fraction $\varphi_{nc} = 0.3$. Inset: Schematic of the parameterized elliptical nanocomposites for micromagnetic simulations; (b) varying φ_{nc} with constant $l_{nc} = 20$ nm; (c) micromagnetic models for $\varphi_{nc} = 0.3$ and $l_{nc} = 20$ nm at specific magnetic fields of H_{ext} equal to (c₁) 0.0 T, (c₂) 0.8 T, (c₃) 5.0 T, (c₄) 6.5 T and (c₅) 8.0 T. Here M_s is valued as the maximum magnetization of each hysteresis.

visual impression of the crystal orientation and phase distribution at the nanoscale. Selected diffraction patterns emphasize partial amorphization of the SmCo_5 phase, showing diffuse rings in contrast to discrete spots for crystalline SmCo_5 and Cu. Dark areas in the phase and orientation map correspond to unindexed regions with low reliability in the analyses, mostly due to amorphization. In the amorphous SmCo_5 phase nanocrystals with approximately 10 to 50 nm in size are embedded. The volume fraction of the nanocrystals was estimated to $\varphi_{nc} = 0.26$ for the sample subjected to 20 rotations.

The amorphous phase is believed to play a crucial role in the saturation behavior of coercivity and possibly also in the further decrease in magnetic hardening with straining. Even though XRD indicates mechanical alloying in the sample subjected to 100 rotations, this is neglected in the following, given that a formation of $\text{SmCo}_{5-x}\text{Cu}_x$ should not lead to the observed decrease in coercivity but rather to an increase [21]. We conducted micromagnetic simulations based on experimental characterization to understand the saturation of coercivity in a sample undergoing 20 rotations. The simulation domains contain an elliptical nanocomposite region (major axis of 900 nm, minor axis of 180 nm, and aspect ratio of 5:1) and a Cu-coated region (thickness of 50 nm), as shown in the inset of Fig. 2a and Fig. S2. SmCo_5 nanocrystals were generated inside the nanocomposite region with controlled size l_{nc} and volume fraction φ_{nc} . Effects of φ_{nc} and l_{nc} on the coercivity were then separately examined. The micromagnetic simulations were carried out by open-source package MuMax³ [22] with numerical details elaborated in Refs. [23,24]. The simulation domains were $1024 \times 512 \times 20$ nm³ in size. Periodic boundary condition (PBC) was applied along the out-of-plane (z) direction by macro geometry approach [25], while Neumann boundary condition was applied on other boundaries [22]. It should be notified that the simulation domain is equivalent to an intersection of a long elliptical cylindrical structure with columnar nanocrystals, where the in-plane domain configuration and domain wall migration are mainly resolved. To reduce the computational consumption, finite difference grids with $1 \times 1 \times 10$ nm³ in size were employed. Further details are summarized in Supplementary Note 2. In order to take numerical fluctuations into account, five cycles of the hysteresis were examined for

each nanostructure, with the averaged one presented in the following contents.

Following the scenario of micromagnetics (with details summarized in Supplementary Note 2), we take the exchange stiffness A_{ex} , the magnetocrystalline anisotropy constant K_u , and saturation magnetization M_s as the main material parameters. These parameters of nanocrystalline SmCo_5 employed in the simulation use the ones measured on bulk material [26,27], which are listed in Table 1. Due to the lack of experimental investigations, the amorphous SmCo_5 phase is assumed to have the identical exchange stiffness A_{ex} and saturation magnetization M_s as the nanocrystalline phase, while its magnetocrystalline anisotropy is assumed to be uniaxial with $K_u^{am} = 0.01K_u$, as also listed in Table 1. This is based on the experimental observations on similar hard magnetic systems, notably amorphous Nd-Fe-B [28–30], where the amorphous phase is treated as a soft magnetic matrix and is generally known to have negligible magnetocrystalline anisotropy [30–32]. The appearance of uniaxial magnetocrystalline anisotropy is due to local internal stresses or induced anisotropy by applied fields, which explains the non-zero K_u^{am} for the amorphous phase. The Bloch domain-wall width is evaluated as $l_{dw} = 2.15$ nm in the nanocrystalline phase and 21.5 nm in the amorphous phase. For the diamagnetic Cu-phase, its magnetization with negative linear-correlation w.r.t. \mathbf{H}_{ext} is modeled with a magnetic susceptibility χ as the modification in free energy density terms is discussed in Supplementary Note 2, though the Cu-phase has a negligible contribution to the magnetization reversal of the whole nanostructures. As unveiled by microstructure analyses in Fig. 1a, SmCo_5 particles are surrounded by Cu-phase, implying a magnetic decoupling among particles.

It is worth noting that the magnetic exchange coupling on the interface inherently differs from the bulk phases, determined by the local structure and chemical component. Such difference further influences the domain wall migration across interfaces. Unfortunately, the modeling of such interface effect remains phenomenological and relies on parameterization, mostly due to limited dimension and difficulties in experimentally determining structure/component of the interfaces. Remarkably, Vansteenkiste et al. formulate the local effective field on in-

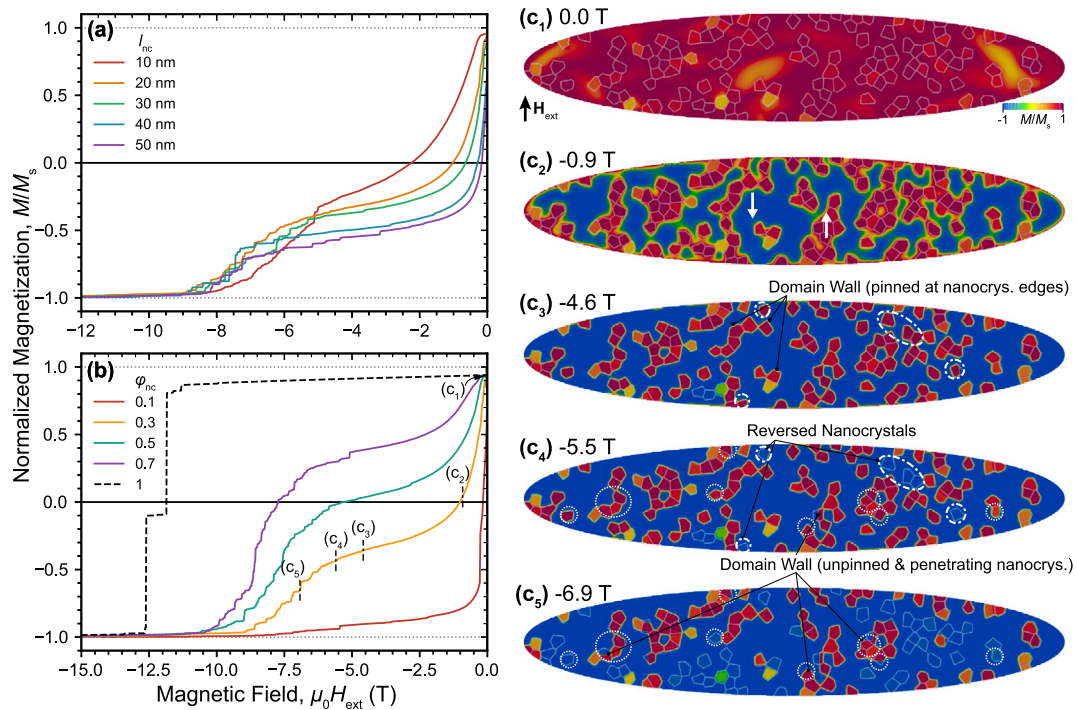


Fig. 3. Simulated second and third quadrant of the hysteresis curves for (a) varying nanocrystallite size l_{nc} with constant volume fraction $\varphi_{nc} = 0.3$; (b) varying φ_{nc} with constant $l_{nc} = 20$ nm; (c) micromagnetic models for $\varphi_{nc} = 0.3$ and $l_{nc} = 20$ nm at specific magnetic fields of H_{ext} equal to (c₁) 0.0 T, (c₂) -0.9 T, (c₃) -4.6 T, (c₄) -5.5 T and (c₅) -6.9 T. Here M_s is valued as the maximum magnetization of each hysteresis.

Table 1
Micromagnetic parameters of corresponding phases.

	A_{ex} (pJ/m)	K_u (MJ/m ³)	M_s (kA/m)	χ
SmCo ₅ (nanocrystal)	8.6	18.3	810.8	-
SmCo ₅ (amorphous)		0.18		
Cu	0	0	0	-6×10^{-5}

interfaces as $\mathbf{H}_{ex}^{intf} = \frac{2S}{\mu_0} \langle A_{ex}/M_s \rangle_H \nabla \cdot \nabla \mathbf{m}$, where $\langle A_{ex}/M_s \rangle_H$ represents the harmonic mean of A_{ex}/M_s of adjacent bulk phases (Eq. 9 of Ref. [22]), and S is a strength factor. It has been shown that the reduced S from one brings extra pinning effects onto the domain wall migration [33], as $S = 1$ can be physically interpreted as a complete atomic contact across the interface [34]. To avoid complexity in the analyses, in this work we took the default $S = 1$ for both nanocrystal-amorphous and inter-nanocrystallite interfaces with assumption of the complete atomic contact, yet understanding the nanoscopic interface exchange coupling should be emphasized and, hopefully, explored in future studies with advanced characterization methods.

Fig. 2a shows the initial magnetization curves for varying nanocrystal size with a constant volume fraction of $\varphi_{nc} = 0.3$ whereas Fig. 2b shows it for varying volume fraction with the constant size of the nanocrystals of $l_{nc} = 20$ nm. To get a precise understanding how the initial magnetization occurs in this microstructure exhibiting an amorphous matrix with embedded nanocrystals, the micromagnetic simulation of the magnetization processes at different external fields are plotted for one specific case of $\varphi_{nc} = 0.3$ and $l_{nc} = 20$ nm in Fig. 2c. In the initial state half of the particle is magnetized upwards and half of it downwards (Fig. 2c).

Fig. 2a and b show that the saturation for all different cases is achieved at $H_{ext} = 13$ T. From the microstructure (Fig. 2c) it is evident that first the amorphous phase turns its magnetization direction towards the external field at very small applied fields before the magnetization of the nanocrystals reverses. The continuous magnetization of the initial curve in the beginning stems from the amorphous phase. At the boundaries of nanocrystals the domain wall gets pinned, which

causes the jumps of the magnetization curve. With increasing external field, the domain wall gets unpinned at the boundaries of the nanocrystals and penetrates those. If the magnetization of a nanocrystal points in the direction of the external field, the domain grows within a group of neighboring crystallites. The jumps originate from single nanocrystals or groups of neighboring nanocrystals which change their magnetization with increasing field.

Fig. 2a indicates a change of the coercivity mechanism with decreasing size of the nanocrystals from nucleation to pinning dominant for $l_{nc} = 10$ nm. The same can be seen in Fig. 2b for a constant size of the nanocrystal $l_{nc} = 20$ nm, when having a fully crystallite particle without an amorphous phase. For small volume fractions of nanocrystals the coercivity mechanism is nucleation controlled and changes to pinning for $\varphi_{nc} = 1.0$. With increasing volume fraction of the crystallites it is also obvious that higher fields are necessary to reach magnetization saturation.

When applying a negative field after saturation, the second and third quadrant of the hysteresis curve is depicted in Fig. 3a for varying nanocrystal size with a constant volume fraction of $\varphi_{nc} = 0.3$. Fig. 3b shows it for varying volume fraction with the constant size of the nanocrystals of $l_{nc} = 20$ nm. The micromagnetic model can be seen again for different applied external field strengths for one specific case of $\varphi_{nc} = 0.3$ and $l_{nc} = 20$ nm in Fig. 3c. Fig. 3a shows that a decreasing size of the nanocrystals leads to an increasing coercivity for a constant volume fraction of nanocrystals, since the number of crystal boundaries increases and hence pinning sites with decreasing size of nanocrystals.

By the aid of the micromagnetic simulations, it is obvious that when applying a negative field after magnetization of the particles (Fig. 3c₁), the magnetization of the amorphous phase rotates at very small negative fields starting at -0.1 T (Fig. 3c₂ for $H_{ext} = -0.9$ T), which corresponds to the smooth decrease of magnetization (Fig. 3a). For the case of $\varphi_{nc} = 0.3$ and $l_{nc} = 20$ nm most nanocrystals do not change their magnetization at a field of -4.6 T, which is already much higher than its coercivity. Until this field, the domain wall is pinned at the nanocrystal boundaries. With further increasing negative field, first nanocrystals change their magnetization, domain walls are unpinned, penetrate into

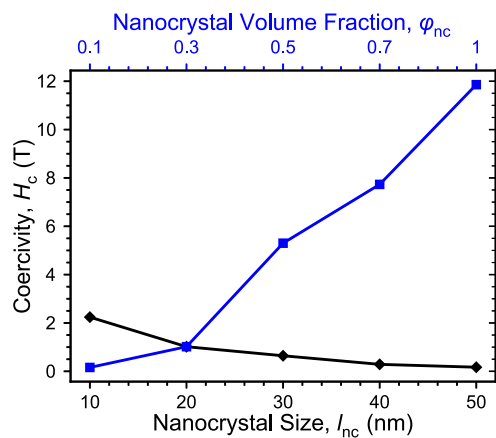


Fig. 4. Simulated coercivity as a function of the nanocrystallite size l_{nc} for a constant volume fraction of $\phi_{nc} = 0.3$, and as a function of the volume fraction ϕ_{nc} for a constant nanocrystallite size $l_{nc} = 20$ nm.

the nanocrystals and align them with the external field. The jumps originate again from single nanocrystals or groups of neighboring nanocrystals which change their magnetization with increasing field in opposite direction. For a constant volume fraction of $\phi_{nc} = 0.3$ a decreasing size of the nanocrystals leads to higher coercivities, but magnetization reversal of the nanocrystals starts at negative fields that are larger than the coercivity for all cases, meaning that the pinning effects on the nanocrystals boundaries have no influence on the coercivity (Fig. 3a). For a constant size of the nanocrystals an increasing volume fraction of the nanocrystals leads to an increasing coercivity (Fig. 3b, Fig. 4). Especially for the case of $\phi_{nc} = 0.7$ the pinning effects on the nanocrystal boundaries lead to increased H_c . The highest coercivity is reached if the particle does not contain amorphous phase $\phi_{nc} = 1.0$, meaning that the amorphous phase is disadvantageous for improving the coercivity due to its significantly lower magnetocrystalline anisotropy (because of the lack of crystallinity) than nanocrystals'.

In Fig. 4 the coercivity is depicted as a function of the volume fraction of the nanocrystals ϕ_{nc} (for constant $l_{nc} = 20$ nm) and as a function of the nanocrystallite size l_{nc} (for constant $\phi_{nc} = 0.3$). It is obvious that the influence of the volume fraction of nanocrystals is much more distinct compared to the influence of the nanocrystallite size. This is due to the fact that the pinning effects of the nanocrystal boundaries for the small volume fractions of nanocrystals only start at external field strengths which are higher than the coercivity.

Comparing the simulated coercivities with the experimental observations, they fit very well. Especially for the nanocrystalline volume fraction of $\phi_{nc} = 0.3$ and a size of the nanocrystals between $l_{nc} = 10$ nm and $l_{nc} = 20$ nm which is in good agreement with the microstructural observations for the small particles made by TEM (Fig. 1c). By the aid of the micromagnetic simulations, the effect of the amorphous phase and the embedded nanocrystals can be understood on a length scale, at which an experimental investigation is very difficult. The simulations show that the amorphous phase is disadvantageous to obtain a high coercivity, and domain wall pinning occurs at the boundaries of the nanocrystals. Except the particle containing large volume fractions of nanocrystals $\phi_{nc} > 0.7$, the pinning at nanocrystal boundaries has no effect on the coercivity since pinning occurs at negative external fields that are larger than the coercivity. Hence, the negative effect of the amorphous phase predominates. The formation of amorphous phase with increasing number of rotations is one reason for the saturation and strong decrease of the coercivity, even though the microstructure gets refined further when subjecting the sample to 100 rotations. The results of the simulations, revealing the negative effect of the amorphous phase, show that the HPT process needs to be adjusted in such a way that the particle size of SmCo_5 is reduced to the single domain region while simultaneously the formation of amorphous phase

is suppressed. One possible process parameter which can be used to adjust the microstructure is the process-temperature which may lead to dynamic crystallization during the process and thus can suppress the formation of amorphous phase. Our micromagnetic simulations provide an understanding of the mechanisms of the saturation behavior of magnetic hardening due to the induced strain by HPT of SmCo_5 -Cu nanocomposites on a length scale that is hard to analyze by experimental investigations and can be used for optimization strategies.

Declaration of competing interest

The authors declare that they have no known competing financial interests or personal relationships that could have appeared to influence the work reported in this paper.

Data availability

The authors declare that the data supporting the findings of this study are available within the paper. The microstructure generation scripts, micromagnetic input files, and utilities are cured in the online dataset (<https://doi.org/10.5281/zenodo.8407722>).

Acknowledgements

Authors acknowledge the financial support of German Research Foundation (DFG) in the framework of the Collaborative Research Centre Transregio 270 (CRC-TRR 270, project number 405553726, sub-projects A01, A06, A08, B04, Z01, Z02, Z-INF). Authors Y.Y., E.F. and B.-X.X. appreciate their access to the Lichtenberg High-Performance Computer and the technique supports from the HHLR, Technical University of Darmstadt, and the GPU Cluster from the sub-project Z-INF of SFB/TRR 270. The computing time on the HPC is granted by the NHR4CES Resource Allocation Board under the project "special00007". Y.Y. also highly thanks Jiajun Sun, Zhejiang University, for his help in the technical check of the micromagnetic simulations. D.N. and L.M.-L. acknowledge the European Research Council (ERC) "Horizon 2020" Program under Grant No. 805359-FOXON and Grant No. 957521-STARE.

Appendix A. Supplementary material

Supplementary material related to this article can be found online at <https://doi.org/10.1016/j.scriptamat.2023.115808>.

References

- [1] O. Gutfleisch, M.A. Willard, E. Brück, C.H. Chen, S.G. Sankar, J.P. Liu, Magnetic materials and devices for the 21st century: stronger, lighter, and more energy efficient, *Adv. Mater.* 23 (2011) 821–842, <https://doi.org/10.1002/adma.201002180>.
- [2] K.P. Skokov, O. Gutfleisch, Heavy rare Earth free, free rare Earth and rare Earth free magnets - vision and reality, *Scr. Mater.* 154 (2018) 289–294, <https://doi.org/10.1016/j.scriptamat.2018.01.032>.
- [3] E.C. Stoner, E.P. Wohlfarth, A mechanism of magnetic hysteresis in heterogeneous alloys, *Philos. Trans. R. Soc. Lond. Ser. A, Math. Phys. Sci.* 240 (1948) 599–642, <https://doi.org/10.1098/rsta.1948.0007>.
- [4] K. Edalati, A. Bachmaier, V.A. Beloshenko, Y. Beygelzimer, V.D. Blank, W.J. Botta, K. Bryła, J. Čížek, S. Divinski, N.A. Enikeev, Y. Estrin, G. Faraji, R.B. Figueiredo, M. Fuji, T. Furuta, T. Grosdidier, J. Gubicza, A. Hohenwarther, Z. Horita, J. Huot, Y. Ikoma, M. Janeček, M. Kawasaki, P. Král, S. Kuramoto, T.G. Langdon, D.R. Leiva, V.I. Levitas, A. Mazilkin, M. Mito, H. Miyamoto, T. Nishizaki, R. Pippin, V.V. Popov, E.N. Popova, G. Purcek, O. Renk, Á. Révész, X. Sauvage, V. Sklenicka, W. Skrotzki, B.B. Straumal, S. Suwas, L.S. Toth, N. Tsuji, R.Z. Valiev, G. Wilde, M.J. Zehetbauer, X. Zhu, Nanomaterials by severe plastic deformation: review of historical developments and recent advances, *Mater. Res. Lett.* 10 (2022) 163–256, <https://doi.org/10.1080/21663831.2022.2029779>.
- [5] R. Pippin, S. Scheriau, A. Taylor, M. Hafok, A. Hohenwarther, A. Bachmaier, Saturation of fragmentation during severe plastic deformation, *Annu. Rev. Mater. Res.* 40 (2010) 319–343, <https://doi.org/10.1146/annurev-matsci-070909-104445>.
- [6] F. Staab, E. Bruder, L. Schäfer, K. Skokov, D. Koch, B. Zingsem, E. Adabifiroozjaji, L. Molina-Luna, O. Gutfleisch, K. Durst, Hard magnetic SmCo_5 -Cu nanocomposites

- produced by severe plastic deformation, *Acta Mater.* 246 (2023) 118709, <https://doi.org/10.1016/j.actamat.2023.118709>.
- [7] L. Weissitsch, M. Stückler, S. Wurster, P. Knoll, H. Krenn, R. Pippan, A. Bachmaier, Strain induced anisotropic magnetic behaviour and exchange coupling effect in Fe-SmCo₅ permanent magnets generated by high pressure torsion, *Crystals* 10 (2020) 1026, <https://doi.org/10.3390/cryst10111026>.
- [8] L. Weissitsch, M. Stückler, S. Wurster, J. Todt, P. Knoll, H. Krenn, R. Pippan, A. Bachmaier, Manufacturing of textured bulk Fe-SmCo₅ magnets by severe plastic deformation, *Nanomaterials* 12 (2022), <https://doi.org/10.3390/nano12060963>.
- [9] L. Weissitsch, F. Staab, K. Durst, A. Bachmaier, Magnetic materials via high-pressure torsion deformation of powders, *Mater. Trans.* (2023), <https://doi.org/10.2320/matertrans.MT-MF2022026>.
- [10] Z.-R. Wang, P.-Z. Si, J. Park, C.-J. Choi, H.-L. Ge, A review of ultrafine-grained magnetic materials prepared by using high-pressure torsion method, *Materials* 15 (2022), <https://doi.org/10.3390/ma15062129>.
- [11] M. Yi, O. Gutfleisch, B.-X. Xu, Micromagnetic simulations on the grain shape effect in nd-fe-b magnets, *J. Appl. Phys.* 120 (2016) 033903.
- [12] M. Duerrschabel, M. Yi, K. Uestuener, M. Liesegang, M. Katter, H.-J. Kleebe, B. Xu, O. Gutfleisch, L. Molina-Luna, Atomic structure and domain wall pinning in samarium-cobalt-based permanent magnets, *Nat. Commun.* 8 (2017) 54.
- [13] S.-K. Kim, S. Hwang, J.-H. Lee, Effect of misalignments of individual grains' easy axis on magnetization-reversal process in granular ndfeb magnets: a finite-element micromagnetic simulation study, *J. Magn. Magn. Mater.* 486 (2019) 165257.
- [14] V. Bautin, A. Seferyan, M. Nesmeyanov, N. Usov, Magnetic properties of polycrystalline cobalt nanoparticles, *AIP Adv.* 7 (2017) 045103.
- [15] K. Hono, H. Sepehri-Amin, Prospect for hre-free high coercivity nd-fe-b permanent magnets, *Scr. Mater.* 151 (2018) 6–13, <https://doi.org/10.1016/j.scriptamat.2018.03.012>, <https://www.sciencedirect.com/science/article/pii/S1359646218301647>.
- [16] A. Kovacs, J. Fischbacher, M. Gusebauer, H. Oezelt, H.C. Herper, O.Y. Vekilova, P. Nieves, S. Arapan, T. Schrefl, Computational design of rare-Earth reduced permanent magnets, *Engineering* 6 (2020) 148–153.
- [17] G. Fuentes, J. Holanda, Y. Guerra, D. Silva, B. Farias, E. Padrón-Hernández, Micromagnetic simulation and the angular dependence of coercivity and remanence for array of polycrystalline nickel nanowires, *J. Magn. Magn. Mater.* 423 (2017) 262–266.
- [18] X. Tang, J. Li, Y. Miyazaki, H. Sepehri-Amin, T. Ohkubo, T. Schrefl, K. Hono, Relationship between the thermal stability of coercivity and the aspect ratio of grains in Nd-Fe-B magnets: experimental and numerical approaches, *Acta Mater.* 183 (2020) 408–417.
- [19] A. Ney, F. Wilhelm, M. Farle, P. Pouloupoulos, P. Srivastava, K. Baberschke, Oscillations of the Curie temperature and interlayer exchange coupling in magnetic trilayers, *Phys. Rev. B* 59 (1999) R3938–R3940, <https://doi.org/10.1103/PhysRevB.59.R3938>.
- [20] O. Gutfleisch, Controlling the properties of high energy density permanent magnetic materials by different processing routes, *J. Phys. D, Appl. Phys.* 33 (2000) R157–R172, <https://doi.org/10.1088/0022-3727/33/17/201>.
- [21] J.C. Téllez-Blanco, R. Grössinger, R. Sato Turtelli, Structure and magnetic properties of SmCo_{5-x}Cu_x alloys, *J. Alloys Compd.* 281 (1998) 1–5, [https://doi.org/10.1016/S0925-8388\(98\)00760-9](https://doi.org/10.1016/S0925-8388(98)00760-9).
- [22] A. Vansteenkiste, J. Leliaert, M. Dvornik, M. Helsen, F. Garcia-Sanchez, B. Van Waeyenberge, The design and verification of mumax3, *AIP Adv.* 4 (2014) 107133.
- [23] L. Exl, S. Bance, F. Reichel, T. Schrefl, H. Peter Stimming, N.J. Mauser, Labonte's method revisited: an effective steepest descent method for micromagnetic energy minimization, *J. Appl. Phys.* 115 (2014) 17D118.
- [24] D. Berkov, K. Ramstöck, A. Hubert, Solving micromagnetic problems. Towards an optimal numerical method, *Phys. Status Solidi A* 137 (1993) 207–225.
- [25] H. Fangohr, G. Bordignon, M. Franchin, A. Knittel, P.A. de Groot, T. Fischbacher, A new approach to (quasi) periodic boundary conditions in micromagnetics: the macrogeometry, *J. Appl. Phys.* 105 (2009) 07D529.
- [26] E. Lectard, C. Allibert, R. Ballou, Saturation magnetization and anisotropy fields in the sm (co_{1-x}cu_x)₅ phases, *J. Appl. Phys.* 75 (1994) 6277–6279.
- [27] J.M. Coey, *Magnetism and Magnetic Materials*, Cambridge University Press, 2010.
- [28] Y. Zhang, W. Li, H. Li, X. Zhang, Coercivity mechanism of α -Fe/NdFe₁₄B nanocomposite magnets with an intergranular amorphous phase, *J. Phys. D, Appl. Phys.* 47 (2013) 015002.
- [29] T. Harada, T. Kuji, K. Fukuoka, Y. Syono, Production of amorphous bulk materials of an Nd₁₅Fe₇₇B₈ magnetic alloy and their magnetic properties, *J. Alloys Compd.* 191 (1993) 255–261.
- [30] H. Kronmüller, B. Gröger, Domains, domain walls and the coercive field of amorphous ferromagnets, *J. Phys.* 42 (1981) 1285–1292.
- [31] H. Kronmüller, et al., *Micromagnetism and the Microstructure of Ferromagnetic Solids*, Cambridge University Press, 2003.
- [32] H. Fujimori, Y. Obi, T. Masumoto, H. Saito, Soft ferromagnetic properties of some amorphous alloys, *Mater. Sci. Eng.* 23 (1976) 281–284.
- [33] J. Leliaert, B. Van de Wiele, A. Vansteenkiste, L. Laurson, G. Durin, L. Dupré, B. Van Waeyenberge, Current-driven domain wall mobility in polycrystalline permalloy nanowires: a numerical study, *J. Appl. Phys.* 115 (2014).
- [34] A. Hernando, I. Navarro, J. González, On the role of intergranular exchange coupling in the magnetization process of permanent-magnet materials, *Europhys. Lett.* 20 (1992) 175.